

Fibre–matrix bond strength studies of glass, ceramic, and metal matrix composites

D. H. GRANDE*, J. F. MANDELL, K. C. C. HONG

Department of Materials Science and Engineering, Massachusetts Institute of Technology, Cambridge, Massachusetts 02139, USA

An indentation test technique for compressively loading the ends of individual fibres to produce debonding has been applied to metal, glass, and glass–ceramic matrix composites; bond strength values at debond initiation are calculated using a finite-element model. Results are correlated with composite longitudinal and interlaminar shear behaviour for carbon and Nicalon fibre-reinforced glasses and glass–ceramics including the effects of matrix modifications, processing conditions, and high-temperature oxidation embrittlement. The data indicate that significant bonding to improve off-axis and shear properties can be tolerated before the longitudinal behaviour becomes brittle. Residual stress and other mechanical bonding effects are important, but improved analyses and multiaxial interfacial failure criteria are needed to adequately interpret bond strength data in terms of composite performance.

1. Introduction

The bond strength between fibres and matrix is an essential property of all composite materials, and considerable resources are being invested in controlling interface or interphase strength and environmental stability in most types of advanced composites. Among the many obstacles to progress in this area has been a lack of adequate experimental techniques for quantitatively determining bond mechanical properties. Additionally, the fundamental relationships between bond chemistry and microstructure, bond mechanical properties and composite performance are not well established. This paper describes an experimental technique and associated analysis which has been used to determine the *in situ* fibre–matrix bond strength in typical as-processed polymer, ceramic, and metal matrix composites. Results are given for several metal, glass, and glass–ceramic matrix composites of current interest, and correlations with composite behaviour are explored in several cases.

1.1. Interface test methods

Provision has been made for adequate fibre–matrix bonding in most established composite systems in the absence of any direct, quantitative measure of bond strength. Judgements as to bond quality are usually based on composite properties or the fractography of failed specimens to observe surfaces and pull-out lengths. However, the complexity of composite mechanical properties and fracture processes makes this an unreliable approach, particularly for systems such as ceramic composites which require bond strength optimization rather than maximization. In a few cases, such as some metal matrix systems [1], it may be possible to observe debond initiation in a conventional composites test such as transverse tension, then

calculate the bond strength from micromechanics; however, for most composite systems a debonding condition for typical interfaces cannot be observed in this manner prior to composite fracture, so that specialized test methods are required.

Several direct approaches have been used to determine the fibre–matrix bond strength in various types of composites. Fibre pull-out tests are possible in cases where an individual fibre can be embedded in matrix in a controlled manner, then tested without breaking the fibre. This is usually limited to materials in which the matrix can be easily cast, as for wires in cement [2], or glass rods in resin discs [3]. Techniques for casting a very thin resin disc [4] or bead [5] around a small-diameter fibre have been successful in a few cases. The pull-out test can be used to determine the bond strength from the stress conditions when debonding initiates, as well as the frictional sliding resistance as the debonded fibre is pulled through the matrix [3]. Pull-out tests are not widely used due to problems with scatter and specimen preparation [4, 5]. Other embedded single-fibre models have been shown to produce bond failures for some material combinations due to Poisson's ratio mismatch or particular shapes [6].

The second major approach is based on the work of Aveston, Cooper and Kelly (ACK) [7]. Their approximate formulations treat multiple cracking in tension of a matrix with more extensible fibres or multiple failure of fibres with a more extensible matrix. In each case, measurements of saturation spacings for fibre breaks or matrix cracks can be used to calculate the load transfer at the interface. The load transfer parameter has been taken as a bond strength in a widely used test developed by Drzal [8] for single fibres in extensible polymer matrices. In brittle-matrix glass and ceramic

*Present address: Boeing Commercial Airplane Co., Seattle, WA 98124, USA.

TABLE I Matrix compositions and properties assumed in analysis and residual stress calculation*

<i>Fibres</i>				
Nicalon $E = 200$; $G = 77$; $\alpha = 32$ (20 to 650°C), 39.3 (20 to 1093°C)				
HMU and P55 carbon [†] $E_z = 379$; $E_r, E_\theta, G_{rz} = 14$; $\nu_{r\theta} = 0.25$; $\nu_{rz} = 0.2$; $\alpha_r = 101$				
<i>Matrices</i> [‡]				
	E_m	G_m	α_m	ΔT
Borosilicate	68	28	32	600
1723 Glass	88	36	52	600
BMAS III	106	43	27	1130
CAS I	88	36	50	1230
LAS III	88	36	15	1030
Aluminium	72	28	240	500
Epoxy	2.8	1.0	650	156
<i>Compositions</i> (major constituents)				
Code 7740 borosilicate glass [26]: B_2O_3, SiO_2				
Code 1723 aluminosilicate glass [26]: Al_2O_3, MgO, CaO, SiO_2				
LAS glass-ceramic [26]: $Li_2O, Al_2O_3, MgO, SiO_2, Nb_2O_5$				
BMAS glass-ceramic [26]: BaO, MgO, Al_2O_3, SiO_2				
CAS glass-ceramic [27]: CaO, Al_2O_3, SiO_2				
Nicalon ceramic-grade fibre [28]: $\beta-SiC, SiO_2, C$				

* Units: E, G : GPa, α : 10^{-7} ($^{\circ}C$)⁻¹, ΔT : $^{\circ}C$ (cooling range from solidification); matrix properties are from Chyung [24] except for epoxy and aluminium. V_f (fibre volume fraction) = 0.35 to 0.40. ν is Poisson's Ratio.

[†] The Hertzian solutions for the transversely isotropic materials and finite-element mesh (FEM) solutions assume the same elastic constants for carbon [25]. All carbon fibres are assumed to have the same elastic constants except for a varying E_z .

[‡] All materials are unidirectional composites; they were supplied by Corning Glass Works except for: carbon-borosilicate (UTRC), carbon-aluminium (DWA Composite Specialties, Inc., Chatsworth, CA, USA).

systems the matrix crack spacing has been correlated with indentation measurements of frictional sliding resistance for Nicalon-LAS (see Table I below) by Marshall [9]. Current efforts at improving the micro-mechanics treatment of cracking problems in ceramic composites should further establish the relationships between matrix cracking and interface properties [10].

A third approach to bond characterization has been indentation tests, where individual fibres [9, 11, 12] or groups of fibres [13] are compressively loaded on a polished surface to produce debonding and/or fibre slippage; these will be described in detail later.

Analysis for most of the bond strength tests has been very limited. The interfacial shear stress, which is usually the parameter of interest, is assumed in most cases to be uniformly distributed along the fibre length. While this assumption may be acceptable for the sliding of an already debonded fibre [11], or where the fibre, matrix, or interphase has yielded, the stress distribution in pull-out or indentation tests is very non-uniform for cases where the materials are elastic and well bonded prior to interface failure. Furthermore, residual stresses from differential thermal expansion, matrix yielding or crystallization shrinkage have not been considered.

1.2. Interface effects on composite properties

The interface plays a critical role in transferring loads throughout a composite, so most composite properties show some bond strength sensitivity. However, several properties are of particular significance for the metal, glass, and ceramic composite systems of interest in this study. Fig. 1 illustrates three critical aspects of composite behaviour which are generally recognized to depend strongly on the interface. In Fig. 1a, the off-axis and shear properties of most composites are expected to correlate directly with bond strength if other parameters are unchanged; empirical correlations are well known for polymer [14] and metal [15] matrix systems, and similar results are found for glass and ceramic matrices [16], as will be described in more detail later. Initial damage in most composites applications occur in this manner, whether in unidirectional or multidirectional materials, so the interface is likely to directly limit the elastic range within which most composites are used in practice.

An equally important factor for glass and ceramic matrix composites in Fig. 1b relates to toughness and flaw tolerance. If the interface is too strong, it is generally recognized [7, 10, 17] that when matrix cracks form normal to the fibres, they will propagate

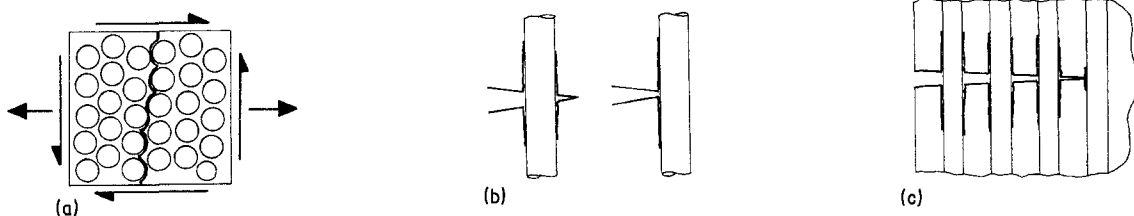


Figure 1 Schematic diagrams of composite properties dominated by the interface: (a) off-axis and shear strength, (b) flaw tolerance (debonding or matrix crack deflection to prevent matrix crack penetration through the fibres), (c) resistance to the onset of macroscopic matrix cracking in longitudinal tension: propagation of matrix crack with bridging fibres.

in a planar mode through the fibres, giving brittle behaviour similar to that in monolithic glasses and ceramics. Behaviour in the desired fibrous, flaw-tolerant manner associated with polymer composites requires that high-modulus, brittle-matrix systems have a sufficiently low bond strength that fibres will debond before cracks propagate through them, or that matrix cracks (or cracks penetrating from off-axis plies) deflect parallel to the fibres as is most often observed with polymer matrices. The need for a strong bond for off-axis and shear properties clearly conflicts with the poorer bonding needed for toughness.

Associated with the debonding requirement in Fig. 1b is the tendency in systems without strong bonding to form matrix cracks normal to the locally debonded fibres in glass and ceramic matrix systems, indicated in Fig. 1c. The stress at which significant matrix cracks form in unidirectional specimens loaded in tension parallel to the fibres limits their practical use conditions (in multidirectional composites it is likely that delamination or cracking in off-axis plies would occur at lower strains than this [18]). As described earlier, the opening of large matrix cracks is resisted in part by work done against friction as the matrix slides relative to the unbroken, bridging fibres [7]. Thus, both the tendency to initiate debonding and the subsequent resistance to sliding of the matrix relative to the fibres appear to be important factors in determining the working stress range of some glass and ceramic matrix materials. Increases in the initial matrix cracking strain consistent with the ACK relationships [7] have been shown for several systems [7, 19].

To summarize, the strength of the interface is expected to play a dominant role in the off-axis and

shear properties, with a higher bond strength giving higher composite strength up to some limit such as the local matrix strength. However, for glass and ceramic matrix composites the longitudinal behaviour may become weak and brittle if the bond strength is too high. The frictional sliding resistance of debonded fibres is of importance in determining the onset of significant matrix cracking in longitudinal tension for some brittle-matrix systems.

2. Test method

The technique used to measure bond strength in this study is based on a microdebonding test method and apparatus developed in several stages for polymer composites [12, 13]. Details of the test procedure and analysis are described elsewhere [12]. Fig. 2 gives schematic diagrams of the apparatus and loading. To determine the bond strength, a selected fibre is loaded in steps of increasing force, with the bond viewed optically between steps, until debonding is observed. The measured debonding force is divided by the fibre cross-sectional area to obtain the average applied compressive stress on the fibre end at debond initiation. The interfacial shear strength is then calculated from the applied stress, using results from the finite-element analysis which will be discussed later.

The microdebonding apparatus in Fig. 2a is configured as a stage in a research-quality optical microscope. The apparatus has one station for loading and a second, optical station for viewing at about $900\times$. At the viewing station fibres are selected for testing, located under a cross-hair and observed after each loading step for evidence of interface failure. Debonding usually appears suddenly over part of the fibre

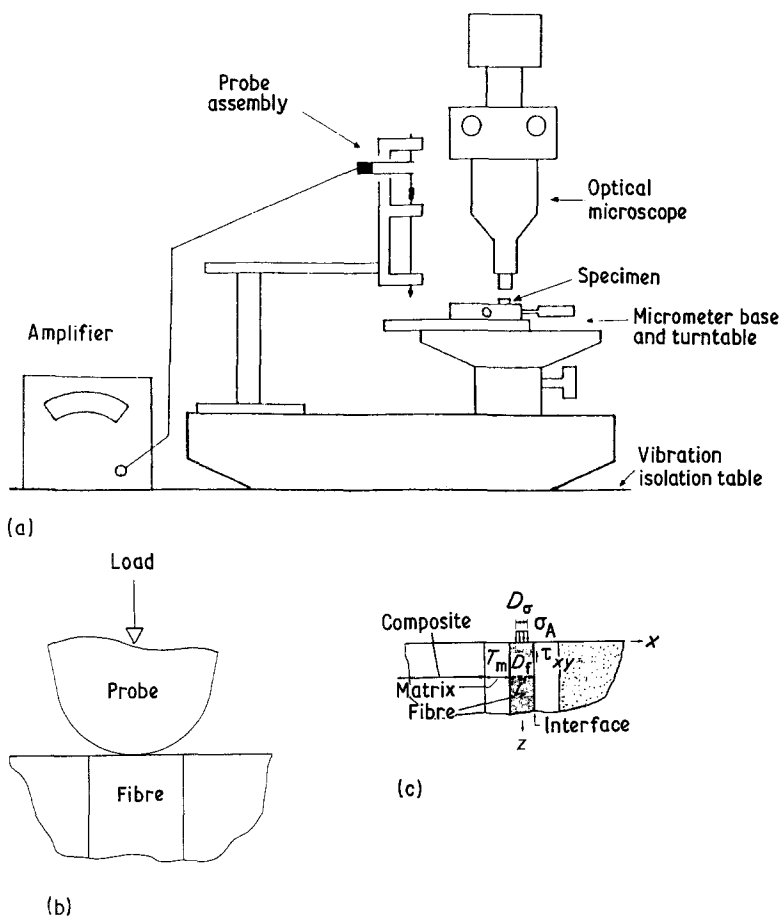


Figure 2 Schematic diagrams of (a) microdebonding apparatus, (b) loading detail, (c) finite-element model for single fibre (from [12]).

circumference at a particular load level. The specimen is on a conventional rotating stage which has been modified with magnetic stops for increased precision in positioning at the viewing and loading stations. The load is applied by raising the specimen against the probe using the microscope focus knob; the applied load is detected with a modified, strain-gauged extensometer which also provides the desired compliance in the load train (about 0.03 mm g^{-1}) for soft contact. The probes used in this study had a ground diamond tip with a radius of about $13 \mu\text{m}$ for Nicalon systems and $10 \mu\text{m}$ for the carbon systems. The load is maintained at the desired level of each loading step for about 5 sec; load increments used here are less than 10% of the total debonding load. The current apparatus allows repeated load positioning within $1 \mu\text{m}$ of the fibre centre, and load increments as small as 0.1 g; vibration isolation of the entire system is essential. Further details of the apparatus may be found elsewhere [12, 20, 21].

Specimen preparation follows conventional metallography techniques, but a smooth surface is essential, and differential wear of the fibres and matrix must be avoided in the final stages. Specimens in this study were polished to $0.25 \mu\text{m}$ diamond grit on a silk cloth in alcohol and lapping oil. Nicalon-LAS III was the only material for which polishing was a problem. The relatively high residual radial tensile stress and the particular interphase characteristics for this system result in chipping and debonding near the interface as the specimen is polished. This problem is reduced with the finest diamond grit in dilute concentrations, so that the interface appeared to be intact for those individual fibres which were selected for testing. How-

ever, further study of specimen preparation methods for the LAS III systems is planned, so that data presented here should be interpreted with caution.

In addition to the bond strength measurement described, a second approach originated by Marshall [9] can be used to determine the frictional sliding resistance between the debonded fibre and the matrix, by applying higher loads and compressing the fibre into the specimen surface. Fig. 3 depicts both modes of loading along with a third, similar method using a thin slice of material as reported for large-diameter filaments by Langhner *et al.* [22]. The thin-slice method is similar to pull-out tests [3], and provides a straightforward interpretation of the behaviour during indentation loading tests: as the load on the fibre is increased, the behaviour is elastic until the bond fails and the force drops to a lower level; further displacement is then resisted by the frictional sliding resistance as the fibre slides relative to the matrix. As with thick specimens, meaningful calculation of the initial bond strength requires a detailed stress analysis due to the very non-uniform elastic stress field, while the frictional sliding stress is usually assumed to be uniformly distributed along the interface. With conventional specimens which are very thick relative to the fibre diameter, the frictional sliding resistance can be calculated following Marshall's original approach [9] using the fibre end displacement determined when the probe contacts the matrix hole circumference (Fig. 3b). The calculation by Marshall [9, 11] requires assumptions as to the lower boundary condition at the end of the debonded length, since the actual debonded length cannot be determined directly. The thin slice has the great advantage for frictional measurements of

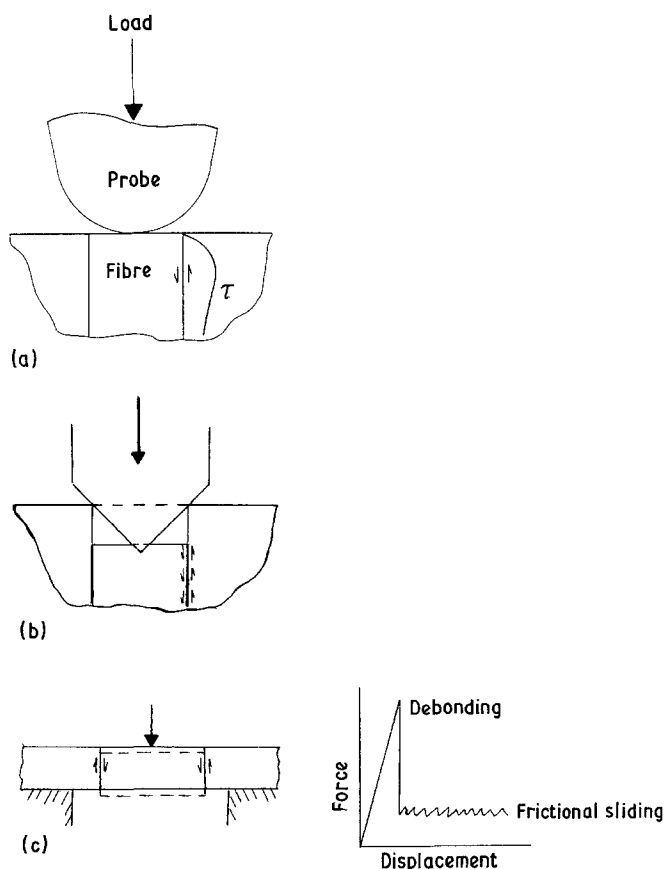


Figure 3 Schematic diagrams of indentation techniques for measuring fibre-matrix bond properties: (a) bond strength calculated from elastic stress field at debond initiation (thick specimen), (b) interface sliding friction after debonding (thick specimen), (c) thin slice.

providing a known debonded length, but sufficiently thin slices are difficult to properly prepare and test for small-diameter fibre systems.

The microdebonding test apparatus in Fig. 2 can be used to determine both the bond strength and frictional sliding resistance as shown in Figs 3a and b. However, the current rounded probe-tip geometry and the absence of accurate probe-displacement measurement reduce the accuracy in the frictional sliding mode as compared with the nanohardness apparatus recently reported by Marshall and Oliver [11]. Most of the results obtained in the present study are for bond strength, and only a few comparisons of frictional sliding resistance will be made.

The interfacial sliding friction, τ_F , given in this study was calculated following Marshall [9] as

$$\tau_F = \sigma_A D_f / 4L_D \quad (1)$$

where $L_D = 2E_f L / \sigma_A$ and L_D is the (calculated) debonding length, L is the distance the fibre was displaced into the matrix, and σ_A is the average stress applied to the fibre end to achieve a displacement L .

3. Analysis

The microdebonding test is run on individual selected fibres on a polished cross-section. The surroundings of

an individual fibre usually include a region of matrix, with neighbouring fibres located at various distances, distributed in a variety of arrangements ranging from close-packed to random and dispersed. A full three-dimensional analysis of the stress field generated by the probe loading would be prohibitively expensive if the actual neighbouring fibres were modelled for each test. Instead, the diameter of the tested fibre and the distance to the nearest-neighbour fibre are recorded for each test on a micrograph, and a very simplified axisymmetric (cylinder) model is used which includes the fibre, surrounding matrix, and average composite properties beyond the matrix. Fig. 2c shows the model geometry, and Fig. 4 gives a typical finite-element mesh arrangement.

Studies of the effects of mesh and overall model geometry as well as the probe-fibre contact problem have been reported [12, 23] for polymer matrix systems. The maximum shear stress along the interface was shown to be insensitive to the area contacted by the probe and to the effective probe stiffness as long as the contact area does not approach the interface. The original finite-element results were encouraging in indicating that the probe contact details should not be a problem, and that specimen surface preparation should not influence the results if failure initiated

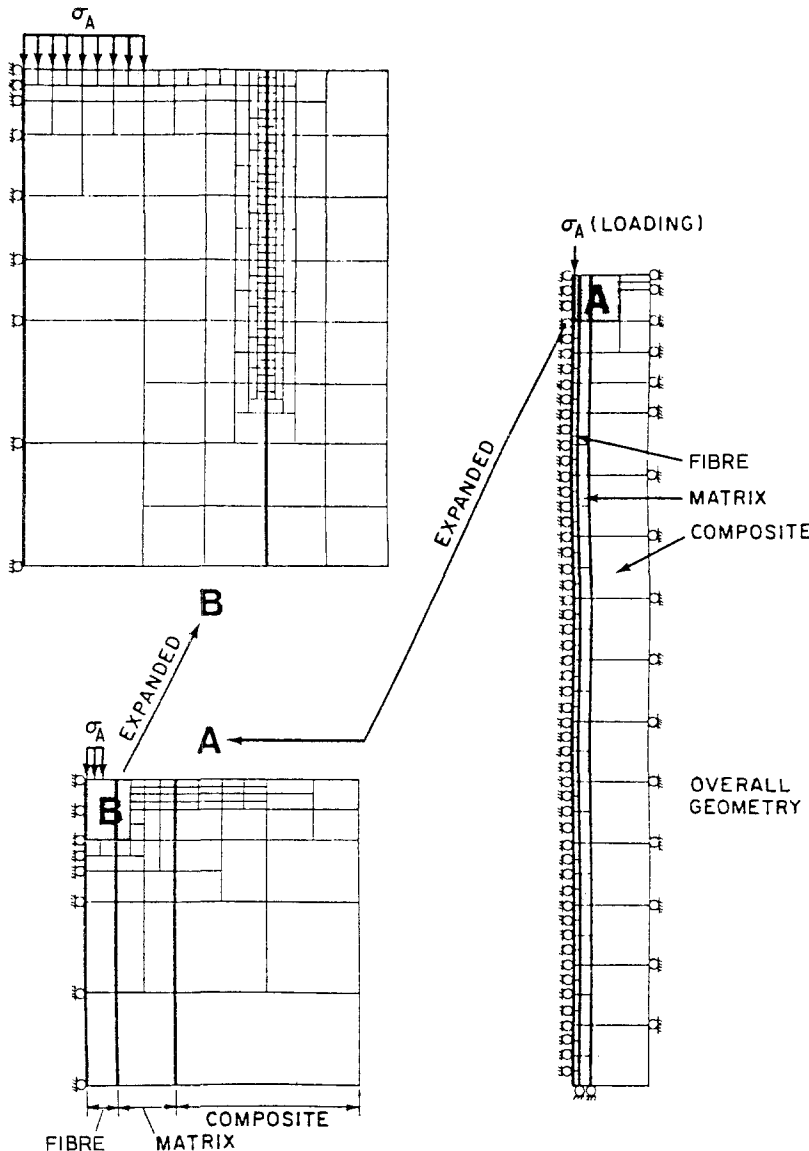


Figure 4 Typical finite-element mesh (from [12]).

below the polished surface at the point of maximum shear stress (Fig. 3a). These observations from the finite-element studies led to the subsequent development of the current microdebonding apparatus [12, 20]. Results for polymer composites obtained with the apparatus generally conformed to expectations based on the finite-element study, with a few exceptions to be discussed later.

Finite-element results have now been obtained using the same analysis for a broader range of material systems, particularly higher-modulus matrices. Figs 5 to 8 give the stress distributions along the interface for four cases with significantly different properties; all of the solutions are for a typical ratio of matrix thickness to fibre diameter, T_m/D_f , of 0.4. The fibre and matrix properties assumed in the analysis are given in Table I, while the composite properties assumed in the far-field were calculated following micromechanics relationships and are given elsewhere [21]. All finite-element results given here assume linear elastic behaviour and do not include thermal residual stresses. The loading in all cases is assumed to be a distributed pressure over the inner 50% of the fibre diameter, while the stresses are normalized in all cases by σ_A , the total probe force divided by the cross-sectional area of the fibre (the average pressure applied to the fibre end).

Fig. 5 gives the test case where the fibre and matrix have the same isotropic elastic constants. The finite-element results are compared with those from the analytical Hertzian solution for a point load on a half-space with imaginary fibre boundaries [29]. The

finite-element results agree well with the Hertzian solution despite the slightly different loading. The results in Fig. 6 are for Nicalon (SiC) fibres in an aluminosilicate glass matrix, and are typical of results for Nicalon fibres in the LAS III, BMAS III and CAS I glass-ceramic matrices. The isotropic Nicalon fibres have an elastic modulus about twice as high as for the matrices, and the stress distributions are very similar to the isotropic homogeneous case in Fig. 5. The normalized stresses in the composites are slightly lower in general, and the radial stress at the free surface appears to remain compressive as compared with a significant tension in Fig. 5. (The results in Figs 5 to 8 are plotted only to the centre of the outer elements at the surface.) In both Figs 5 and 6 the maximum shear stress occurs at a distance of about $0.4D_f$ below the surface, while the radial stress in this region is compressive and of a similar magnitude to the shear stress. It is anticipated that debonding will occur in the Nicalon systems at the point of maximum shear stress, and that the radial compressive stress may be high enough to strongly affect the bond strength.

Figs 7 and 8 show major differences in the stress distributions for glass and epoxy matrices reinforced with carbon fibres. The carbon fibres are assumed to be transversely isotropic with the elastic constants given in Table I, and the carbon-glass results are very similar to those for carbon-aluminium. Comparison of Figs 6 and 7 for similar glass matrices but with Nicalon and carbon fibres shows that the directional properties of the carbon fibres significantly reduce

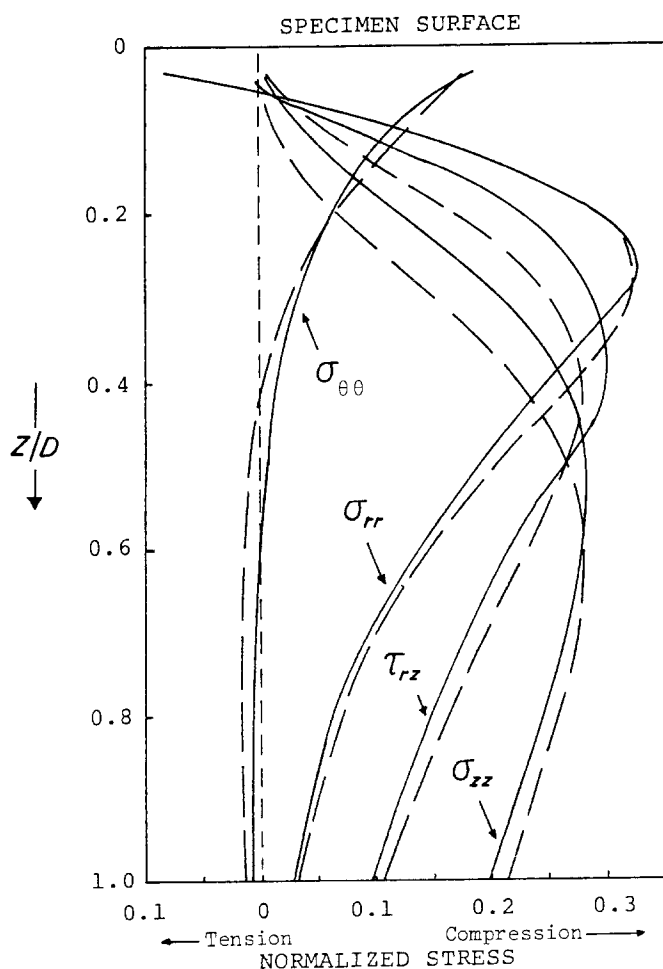


Figure 5 Stress components along imaginary interface normal to a free surface in homogeneous, isotropic material; comparison of (—) Hertzian point-load solution with (---) finite-element results. (Z is the coordinate; D is the fibre diameter.)

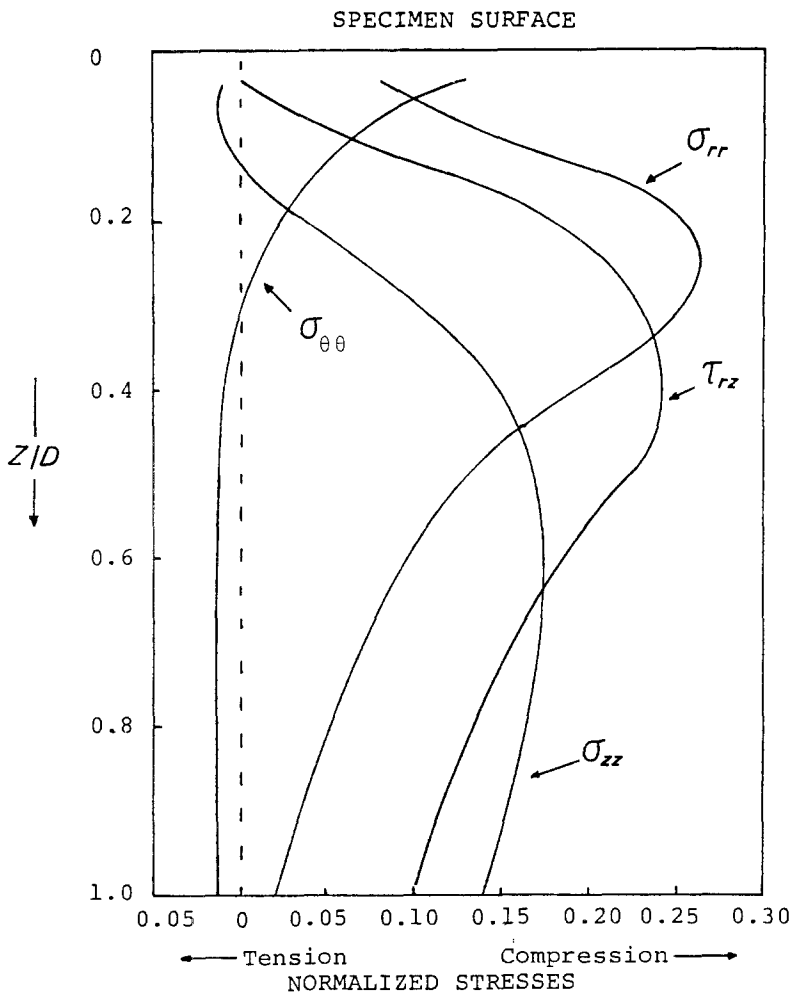


Figure 6 Interfacial stress components for Nicalon ceramic fibre-1723 glass matrix system.

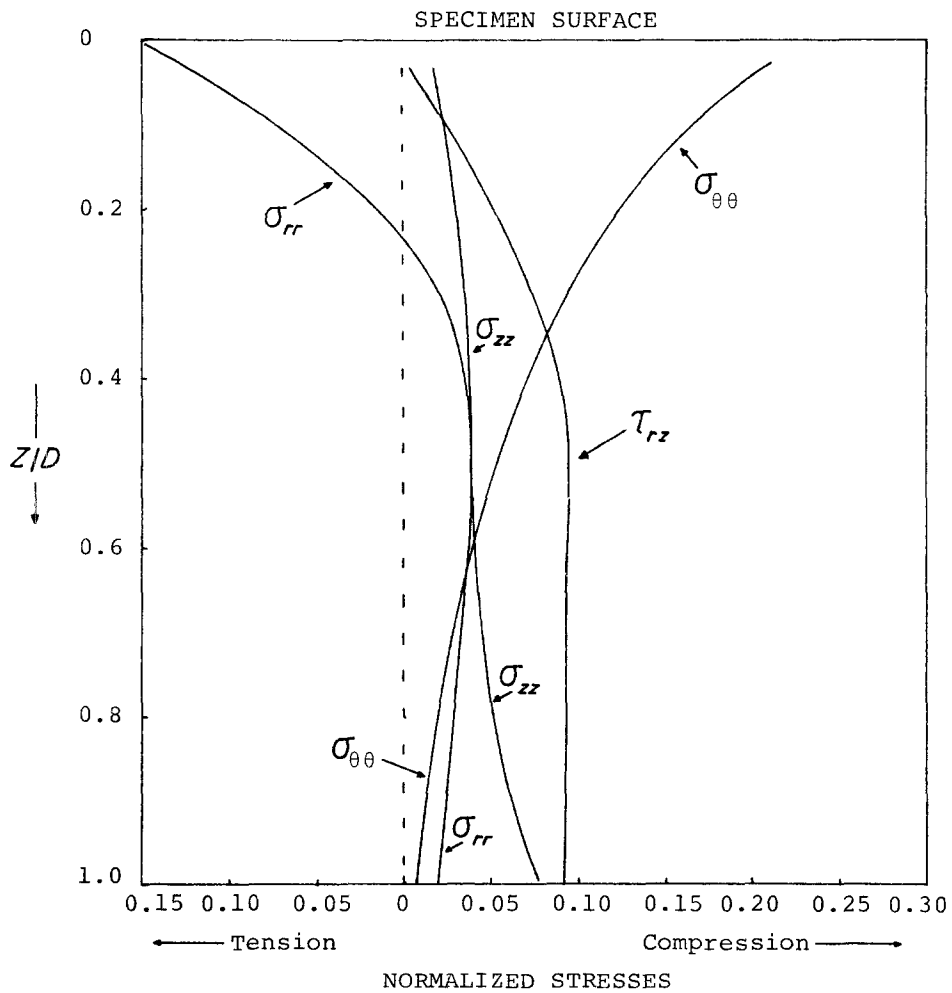


Figure 7 Interfacial stress components for HMU carbon fibre-borosilicate glass matrix system.

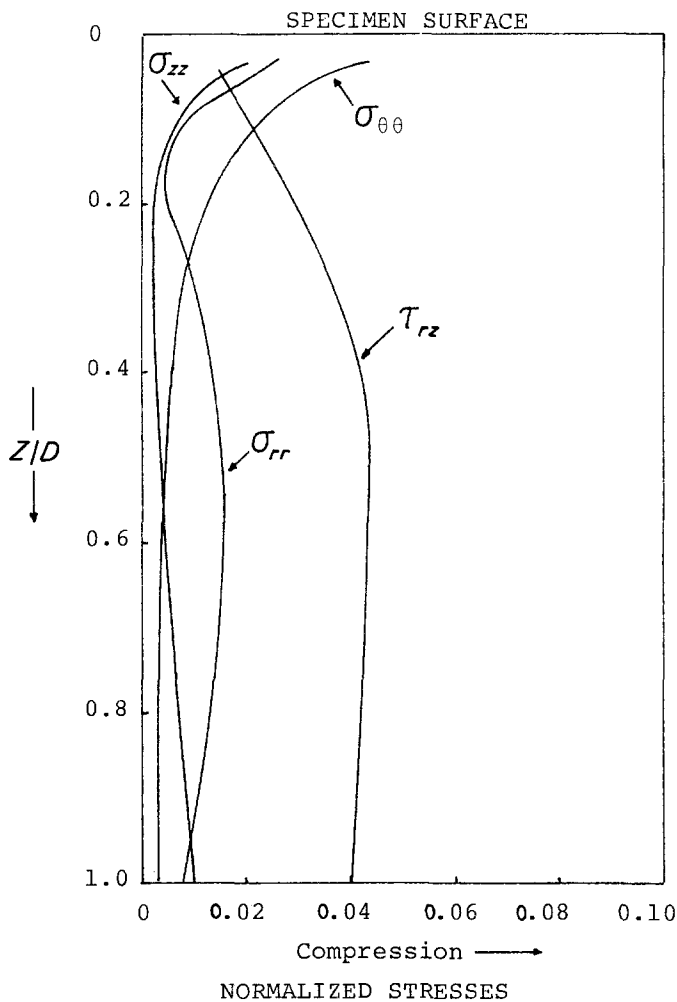


Figure 8 Interfacial stress components for carbon fibre-epoxy matrix system.

most of the stress components, and spread out the stress transfer process further along the fibre length. A low-modulus matrix like epoxy has a similar effect with isotropic fibres [12] as well as with carbon fibres (Fig. 8, note expanded scale). The stresses for carbon-epoxy are uniformly lower than those for the carbon-glass in Fig. 7. The maximum radial compression is significantly lower than the maximum shear stress for both carbon fibre systems, but in the carbon-glass a radial tensile stress appears as the free surface is approached. A tensile component at the surface is generally noted when the matrix modulus exceeds the fibre radial modulus.

The radial tensile stress component near the free surface has been used as a failure criterion for debonding in carbon fibre systems with high matrix moduli, including glass and aluminium. However, further

refinements in the analysis are required to adequately treat the free-surface problem, and the accuracy of stresses in this area is uncertain. Of even greater uncertainty is the effect of thermal and other residual stresses which are not included in these results, but are expected to be very significant near the free surface based on preliminary finite-element results obtained for several cases. Data which are likely to be most strongly affected by residual stresses will be noted as they appear.

The effect of fibre spacing on the experimental results was not accurately predicted by the finite-element model for polymer composites, and an empirical correction was used to account for the moderate-spacing effect [12]. This appears to be much less of a problem for higher modulus matrices as indicated in Table II. The maximum shear stress is affected much less by changes in the matrix layer thickness for all the higher modulus systems as compared with E-glass or carbon-epoxy. For convenience, the fibre spacing has been ignored for the data presented in this paper, and a typical value of 0.4 for T_m/D_f is assumed.

Despite uncertainties about residual stresses and radial tension in some cases, results for the normalized maximum interfacial shear stress, τ_{max}/σ_A , are given as a function of G_m/E_f (matrix shear modulus/fibre axial modulus) for a variety of material systems in Fig. 9, and these values are used to reduce the experimental data for the various material systems. The upper line is fitted to data for isotropic fibres with various isotropic matrices. Approximate shear-lag analyses [12] predict a linearly increasing τ_{max} with $(G_m/E_f)^{1/2}$ as the

TABLE II Effect of fibre spacing on maximum normalized interfacial shear stress from finite-element analysis

Composite system	$(G_m/E_f)^{1/2}$	Maximum normalized shear stress, τ_{max}/σ_A		
		T_m/D_f		
		0.10	0.40	1.0
Carbon-epoxy	0.062	0.060	0.043	0.034
E-glass-epoxy	0.124	0.133	0.098	0.073
Nicalon-1723	0.422	0.275	0.246	0.219
Nicalon-BMAS	0.462	0.286	0.260	0.232
HMU carbon-borosilicate	0.274	0.108	0.094	0.090
P55 carbon-aluminium	0.275	0.101	0.092	0.088
Hertzian isotropic	0.620	(0.279)		

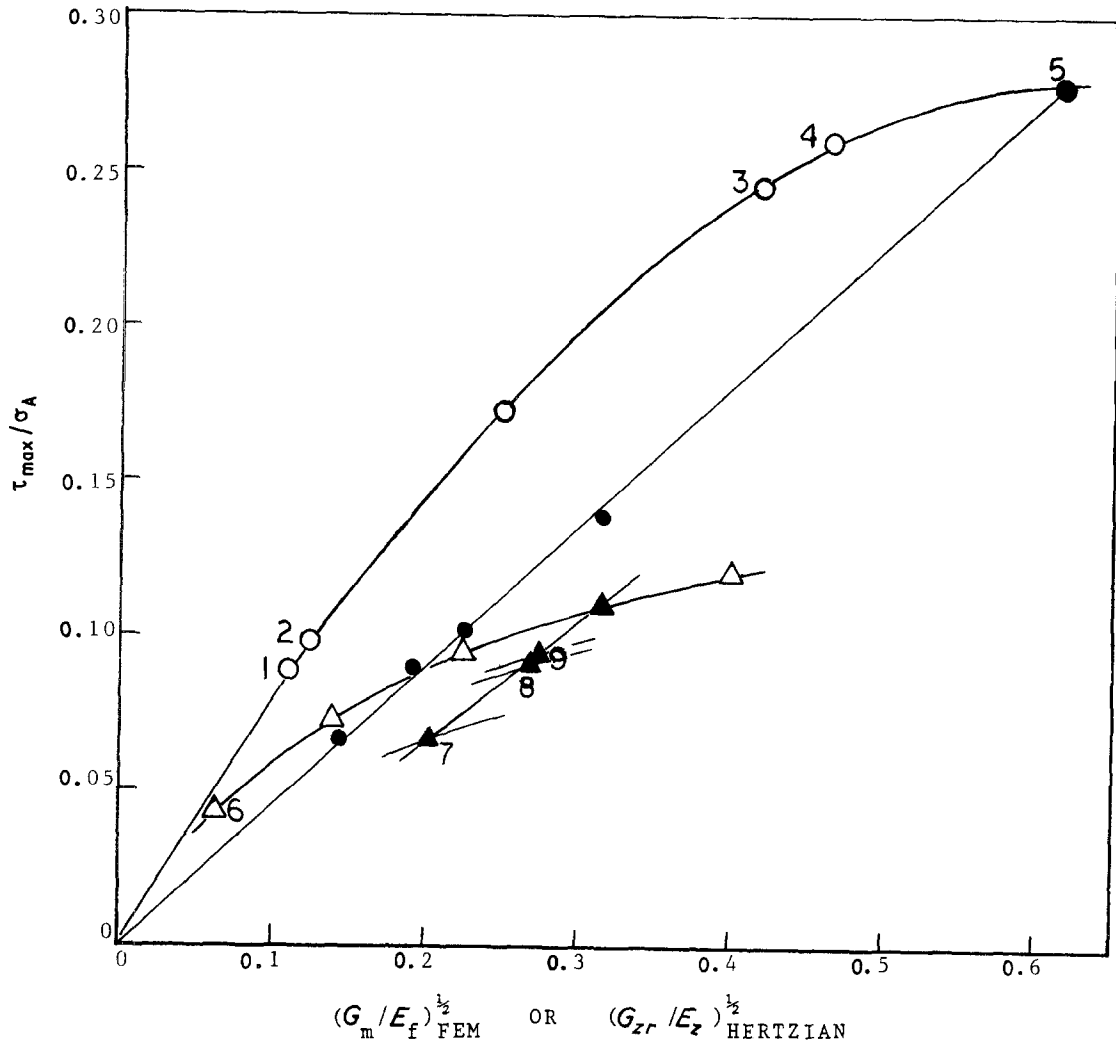
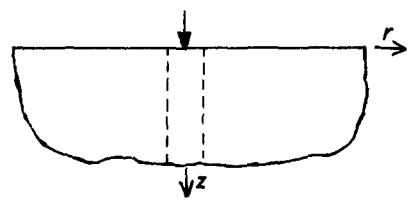
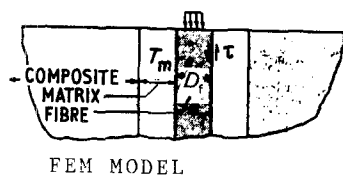


Figure 9 Maximum normalized interfacial shear stress plotted against $(G_m/E_f)^{1/2}$ for various actual and hypothetical material systems and trends from Hertzian solutions for transversely isotropic properties referenced to an imaginary interface position. (○) FEM model, isotropic fibres; (●) Hertzian with $G_{zr} = 14$ MPa, E_z varying; (△) FEM with $E_z = 276$ GPa, matrix varying; (▲) FEM with $G_m = 28$ GPa, carbon fibre E_z varying. (1) S-glass-epoxy, (2) E-glass-epoxy, (3) Nicalon-1723 glass, (4) Nicalon-BMAS, (5) Hertzian isotropic, (6) carbon-epoxy, (7) P100-aluminium, (8) P55-aluminium, (9) HMU-borosilicate.

matrix increases in relative stiffness, which is approximately true for the three epoxy matrix cases. However, as the matrix shear modulus approaches that of the fibre, the relationship becomes non-linear, eventually approaching the Hertzian homogeneous isotropic solution asymptotically. The curve with open triangles is for a carbon fibre with 276 GPa axial modulus with varying matrix moduli (the same off-axis properties are assumed for all carbon materials, Table I). As G_m increases, the directional carbon fibre properties greatly reduce the maximum shear stress relative to that for isotropic fibres. Higher-modulus carbon fibres (Nos 7, 8 and 9) with the same 28 GPa matrix shear modulus (equal to the assumed fibre G_{zr}) show a further decrease in τ_{max} as the axial fibre modulus increases (other fibre elastic properties are kept constant). The reduction in τ_{max} due to the carbon fibre

elastic constants is similar to that obtained for a Hertzian point load on a homogeneous, transversely isotropic half-space [30] shown by the closed circles. The transversely isotropic elastic constants result in a distortion of the stress field along the fibre axis which is retained in composites with relatively stiff matrices.

Calculations of the bond strength in this study assume either a maximum interfacial shear stress criterion or a maximum radial tensile stress criterion, ignoring other stress components and residual stresses in both cases. The interfacial shear strength, τ_{DEB} , is calculated from

$$\tau_{DEB} = \sigma_{DEB}(\tau_{max}/\sigma_A)_{FEM} \quad (2)$$

where σ_{DEB} is the average pressure applied to the fibre end at debonding, and $(\tau_{max}/\sigma_A)_{FEM}$ is the ratio of the maximum shear stress to applied pressure from Fig. 9.

TABLE III Interfacial shear strength and sliding friction for Nicalon-reinforced glass and glass–ceramics

Matrix	Interfacial shear strength (MPa)		Sliding friction, average (MPa)
	Average	S.D.	
1723 glass (alumino–silicate)	236	38.6	143*
LAS III	56	22.5	3.2
BMAS III	60	11.7	5.5
CAS I	249	39.3	–

*Calculation invalid; sliding friction calculated from matrix crack spacing in tension gives 6.9 MPa.

For cases with a tensile radial stress at the surface, the interfacial tensile strength was calculated from

$$\sigma_{DEB}^r = \sigma_{DEB}(\sigma_{max}^r/\sigma_A)_{FEM} \quad (3)$$

where $(\sigma_{max}^r/\sigma_A)_{FEM}$ is the ratio from the FEM analysis of the maximum radial tensile stress (at the surface) to the applied pressure. In all cases the FEM results are for a ratio of matrix layer thickness to fibre diameter of 0.40.

4. Experimental results and discussion

4.1. Results for control samples

Tables III and IV list bond strength results for as-received control samples of materials used in this study, tested under ambient conditions; fibre and matrix compositions and properties are identified in Table I. The only significant experimental problems in running the tests were with polishing of the Nicalon–LAS III as described earlier, and with some systems discussed later which had bond strengths of 800 MPa or more. Fibres can crack under the probe if the bond strength is very high or if the fibre has weak directions, as with carbon. Splitting of carbon fibres is a problem if very small probe tip radii are used, but few problems were encountered with tip radii of 10 μ m or more. Standard deviations for most cases were 10 to 20% of the mean, which is not significantly higher than for most macroscopic composite properties; the higher scatter for Nicalon–LAS III may reflect the surface preparation difficulties. At least 10 tests were run for each case.

Data for the Nicalon systems in Table III show several interesting effects. All systems are determined to have a significant bond strength. The two systems with lower bond strength, LAS III and BMAS III, have relatively low matrix thermal expansion coefficients, while the two systems with high bond strength have high matrix expansion coefficients, as will be discussed in more detail later. All of these materials have a high radial compressive stress in the region of

maximum shear stress, as shown in Fig. 6; this may be increased or decreased by residual stresses depending on the system. The compressive radial stresses from the combined mechanical and thermal residual effects are expected to increase the resistance to bond failure in shear, but multiaxial failure criteria are not yet available.

Despite the wide range of measured bond strength values for the four Nicalon fibre systems, all have relatively high longitudinal composite flexural strengths exceeding 750 MPa [24]. The mechanical properties of the LAS III [31] and 1723 [18, 21] composites have been studied in greater detail, and both show longitudinal tensile strengths exceeding 700 MPa and strains at failure exceeding 1%. Fibre pull-out lengths on the fracture surface for the LAS III systems ($> 50D_f$ [28]) are much greater than for the 1723 system (10 to $20D_f$ [18]), reflecting the different bond properties and residual stresses, but having little influence on the longitudinal strength or toughness.

Interfacial sliding friction values for three of the Nicalon systems are also given in Table III, calculated from Equation 1. The value for the LAS III material is close to that reported by Marshall [9], and the BMAS III is in a similar range. The frictional value calculated for the 1723 system is very high, but it is not valid since it violates the assumptions inherent in Equation 1 due to the high bond strength and short apparent debonding length [11]. A value of frictional sliding resistance for the 1723 system calculated following Aveston *et al.* [7] from the saturation matrix crack spacing in tension of 100 μ m [18] is about 7 MPa, much lower than that in Table III. Similar calculations from matrix crack spacing for LAS III [9, 32] are in agreement with the indentation-derived frictional values. These results suggest either that frictional sliding resistance is strongly affected by the stress field difference at matrix cracks, or else that severe problems exist with indentation friction measurements for systems like the 1723 glass having a high matrix thermal expansion coefficient. Indentation tests with very thin slices might resolve this discrepancy by providing a more meaningful value of sliding friction using the known debond length. The high indentation friction value calculated here for the 1723 system could be due entirely to a high bond strength at the lower boundary of the debonded length, which is assumed to be zero in Equation 1 [11].

Bond strength values calculated for the carbon-fibre systems in Table IV appear to be dominated by the radial tensile stress at the surface except for the typical epoxy matrix system. Detailed interpretation of the results for the aluminium and glass matrices is not

TABLE IV Interfacial shear and tensile stresses at debonding for carbon fibre composites

Material	Maximum interfacial shear stress (MPa)		Radial tension at surface (MPa)	
	Average	S.D.	Average	S.D.
Carbon–epoxy [12]	44.0	5.7	–	–
HMU–borosilicate	10.2	2.3	17.3	3.9
P55–6061 aluminium	39.3	14.1	68.8	24.7
P55–2024 aluminium	27.9	5.3	48.8	9.3

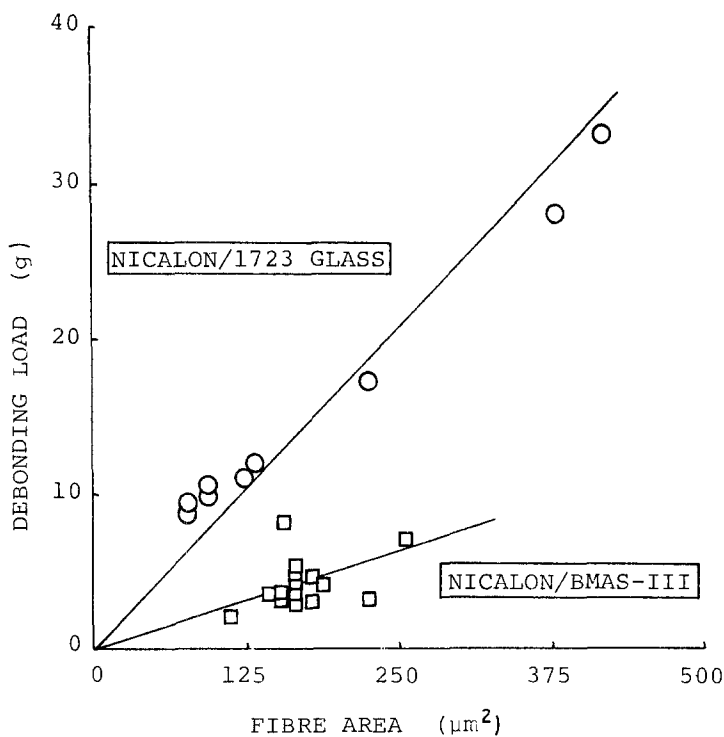


Figure 10 Raw data for debonding load plotted against fibre cross-sectional area for (○) Nicalon-1723 glass, (□) Nicalon-BMAS III. Straight lines indicate trends for a constant calculated bond strength (independent of diameter).

justified until the apparently high free-surface residual thermal stresses are included in the analysis, and non-linear yielding effects may also be important with the aluminium matrix systems. The probable importance of residual stresses for these systems as well as the Nicalon-LAS III is evident in very preliminary finite-element runs which include thermal effects.

Fig. 10 gives raw debonding force data as a function of fibre cross-sectional area, A_f , for the Nicalon-BMAS III and 1723 materials. It is implicit in the data reduction scheme that the debonding force should scale with A_f , giving a constant σ_A at debonding. This is strongly violated with polymer matrices for very closely spaced fibres, while fibres greater than $0.3D_f$ apart typically follow the expected trend [21]. The very limited data for the systems in Fig. 10 are plotted without regard to fibre spacing, and show a variation with A_f which is in better agreement with the linear prediction than was found with carbon-epoxy [21]. Thus, the effects of fibre spacing appear to be much less significant for the higher-modulus composites, as predicted by the finite-element results (Table II). The raw data trends tend to justify the very simplified data reduction scheme used in this study, but further analysis and testing are currently being pursued. Those systems with greater residual stress effects are also expected to show a more significant influence of near-neighbour fibres, but this has not yet been empirically established.

4.2. Effects of processing temperature

It was noted earlier that the longitudinal behaviour of glass and ceramic matrix composites is expected to become weak and brittle if the bond strength is too high. This general perception has been confirmed quantitatively in a series of Nicalon-1723 glass matrix samples which were processed at various temperatures, supplied by Corning Glass Works. Like other successful Nicalon-reinforced glass and glass-ceramic

composites, this system has been reported to form a 10 to 20 nm thick carbon-rich layer at the interface if the processing temperature is sufficiently high [28, 33].

Fig. 11 gives Corning data [24] for the longitudinal flexural strength as a function of processing temperature, together with results for the bond strength. At low processing temperatures an adequate carbon layer does not form [33] and the bond strength is very high, in some cases beyond the capacity of the microdebonding apparatus; the flexural strength is very low, and the composite behaviour is brittle under these conditions. At processing temperatures between 900 and 1000°C the flexural strength is only slightly higher and the behaviour relatively brittle, despite the fact that most of the interfaces have dropped to a much lower strength. However, some localized regions of very high bond strength are still found, usually on the order of 1 mm² or less in extent, and these regions cause the poor composite behaviour. Processing temperatures of 1100°C and above result in the generation of 10 to 20 nm thick carbon layers and uniform bond strengths below 300 MPa. The composites are strong and tough, showing fibrous fracture surfaces [33]. The moderate-reduction in flexural strength at the highest processing temperature probably results from fibre degradation during processing. The effects shown in Fig. 11 are due to changes in chemical bonding, since the matrix coefficient of expansion is not changed by altering the processing temperature. The results confirm that very high bond strengths do cause weak, brittle behaviour, but it is also evident that excellent behaviour can be obtained with bond strengths as measured in the microdebonding test which are very substantial in magnitude.

4.3. Embrittlement at high test temperatures

In elevated-temperature mechanical tests in air it has been widely reported that Nicalon-glass-ceramic systems develop a brittle, flat fracture region near

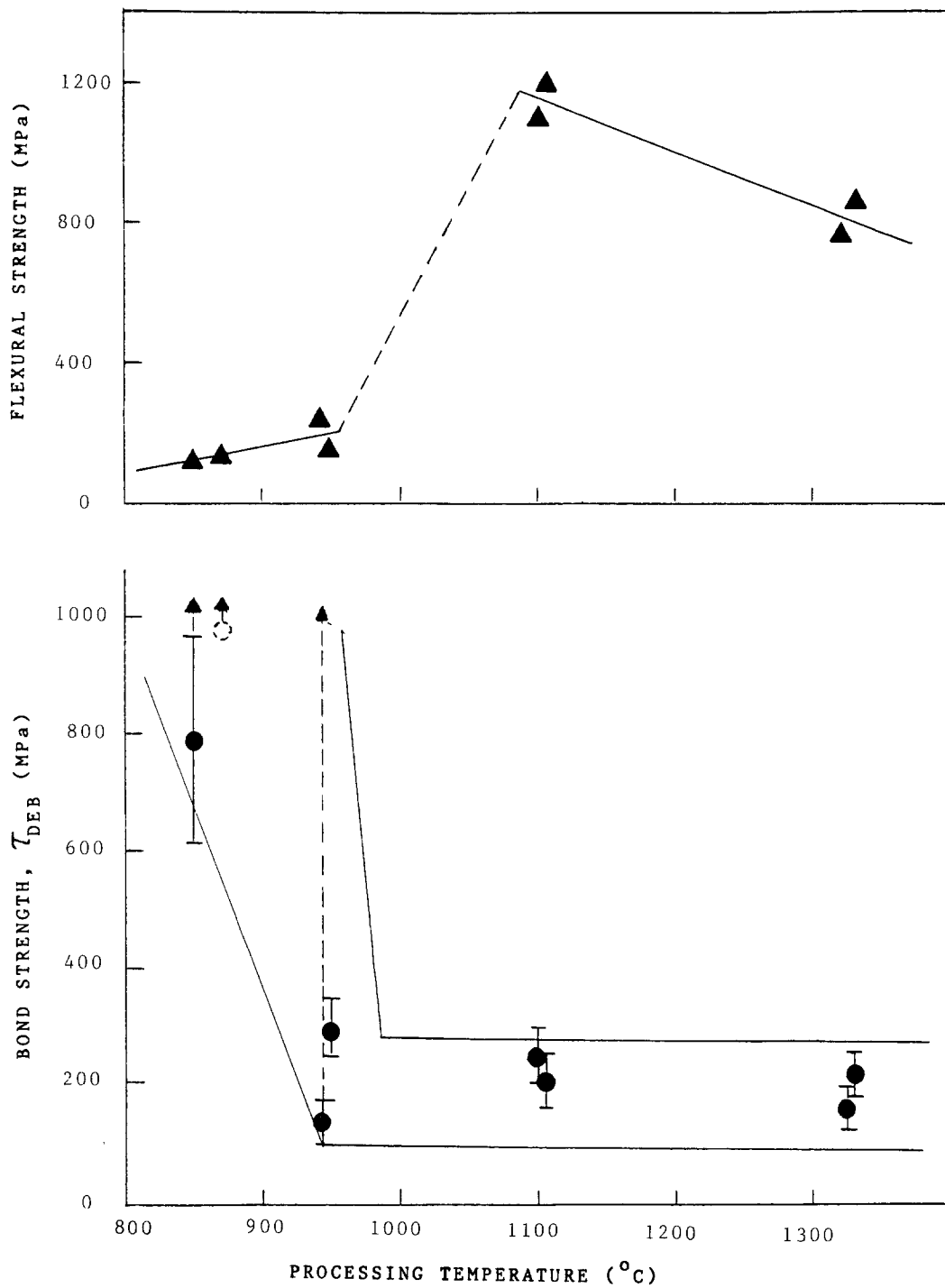


Figure 11 Correlation of (●) bond strength and (▲) composite flexural strength for Nicalon-1723 processed at different temperatures. Vertical arrows indicate that some fibres had $\tau_{DEB} > 800$ MPa; bars show standard deviations for tested fibres only.

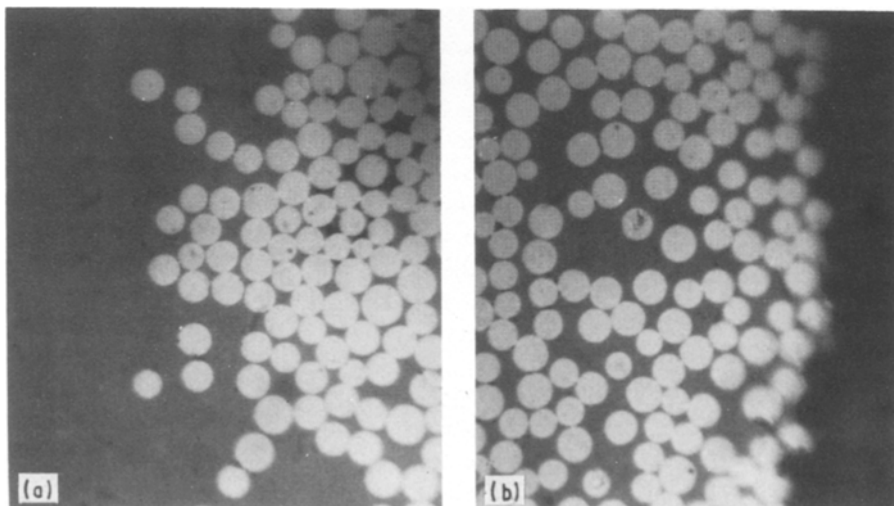


Figure 12 Cross-section of Nicalon-BMAS III block conditioned for 12 h at 1000°C in air prior to sectioning, showing (a) as-moulded surface and (b) ground surface (average $D_f = 13.5 \mu\text{m}$).

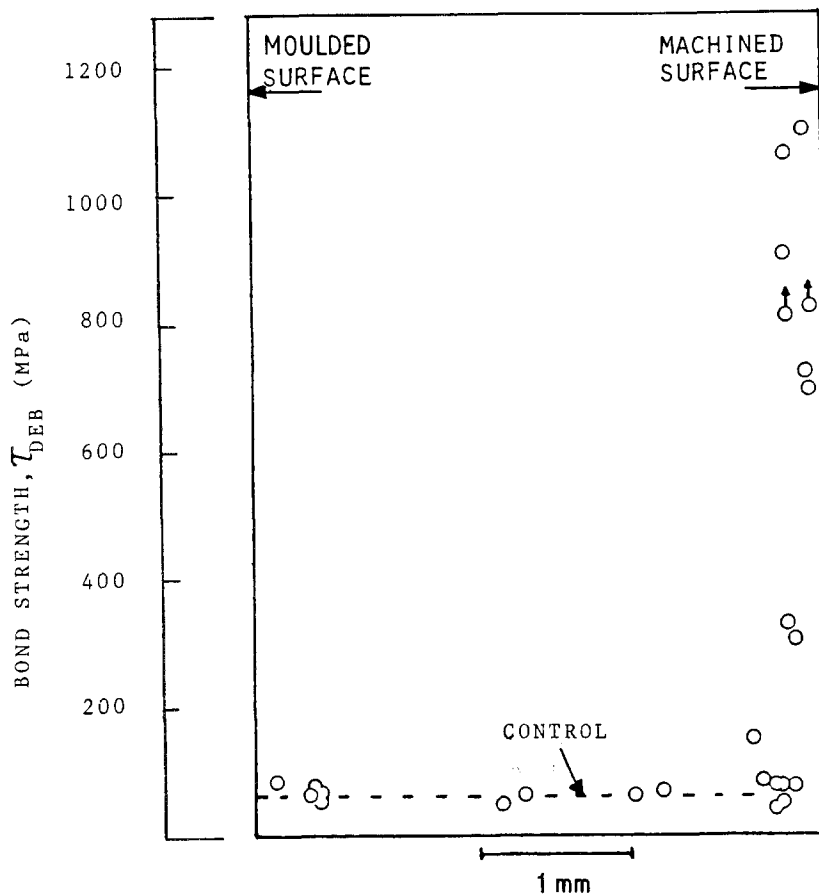


Figure 13 Bond strength across the cross-section of the specimen in Fig. 12 (from [18]).

exposed tensile surfaces in the 1000°C temperature range [18, 28, 34, 35]. The origin of this embrittlement has been associated with oxidation [36] of the carbon interface layer leading to fibre degradation and/or the formation of a strong bond at the interface [28, 34]. The Nicalon-BMAS system shows the embrittlement effect, which causes a loss in tensile and flexural strength and failure strain [18, 28]; the formation of a new bridging interphase layer after oxidation of the carbon layer has been reported [28].

The embrittlement effect has been investigated for Nicalon-BMAS by determining the bond strength distribution through the thickness after exposure. In the first example, a block of material was conditioned with one as-moulded surface (with a glass layer outside the matrix and fibres) and the other surface ground with a 300 grit diamond wheel, as shown in Fig. 12. After conditioning for 12 h at 1000°C in air the block was sectioned, and the bond strength measured across the section. Fig. 13 indicates that the fibres on the protected as-moulded surface and on the interior did not change in bond strength from the as-received control material. However, the bond strength increased dramatically as the ground surface was approached, reaching levels beyond the capacity of the apparatus in some cases. The depth of penetration of the oxidation effect varied from location to location, and Fig. 13 is a summary of all measurements. No microcracking was observed beyond about the first layer of fibres, so it appears that the oxidation spreads from fibre to fibre at points of near-contact, as well as along the fibres. Tests near the exposed end of a specimen conditioned for 3 h at 1000°C showed high bond strengths across the entire cross-section at a tested depth of about 0.5 mm from the exposed surface,

but the depth of oxidation tunnelling along the fibres has not been explored in detail.

Similar data are given in Fig. 14 for a tensile specimen tested to failure at 1000°C, which showed an embrittled surface layer [18] (the data are from a cross-section away from the fracture surface). The specimen (with ground surfaces) was at the test temperature for about 3 h prior to testing, and shows a similar depth of penetration of the oxidation effect to Fig. 13; the depth of the brittle layer was also of similar magnitude. No significant bond strength changes were found in specimens tested at 600 and 800°C after conditioning for 3 h. Efforts to measure the frictional sliding resistance of fibres in the oxidized zone were not successful due to the same high bond strength and short debonded length problems discussed earlier for Nicalon-1723.

The oxidation embrittlement results are consistent with those from low processing temperatures with Nicalon-1723. In both cases very high bond strengths, exceeding 500 MPa in many cases, gave rise to brittle composite behaviour. Under these conditions, the first significant matrix crack to form propagates through the composite, breaking the fibres and causing brittle fracture. This is not observed when the bond strengths uniformly measure below 300 MPa. The applicability of the high-temperature embrittlement findings to other matrix systems is uncertain. Microscopy studies of oxidized interfaces in Nicalon-LAS III have not shown a clear formation of new bridging material after removal of the carbon as found with BMAS III [28]. Efforts to determine the sliding resistance of oxidized Nicalon-LAS III have shown higher forces but a dependence on exposure conditions [37].

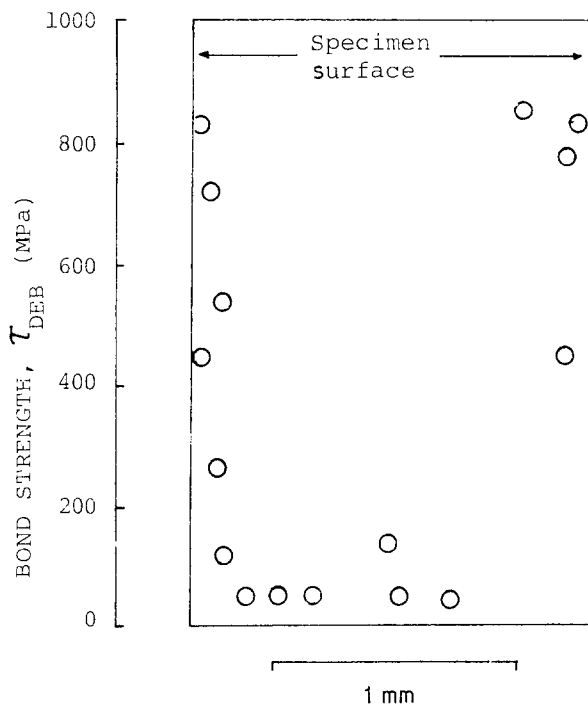


Figure 14 Bond strength against distance through the thickness of unidirectional Nicalon-BMAS III specimen tensile tested in air at 1000°C.

4.4. Effects of matrix modification

The bond strength values given in Table IV for carbon-borosilicate glass material are low, and efforts have been made to increase bonding by modification of the matrix. Samples from the study reported in [19] were supplied by United Technologies Research Center (East Hartford, Connecticut) with a control composition (Code 7740 borosilicate, but without Al_2O_3) and with additions of Al_2O_3 , Nb_2O_5 , and MoO_3 . Fig. 15 gives bond strength values obtained on these systems (both τ_{DEB} and σ_{DEB}^r) plotted against composite interlaminar shear strength data supplied by United Technologies (other data for these systems are given by Prewo and Nardone [19]). The results indicate a substantial increase in bond strength for several of the matrix additions. The bond strength increases also appear to have increased the composite shear strength, but considerable scatter is evident. As noted earlier, thermal residual stresses near the free surface are likely to have a major effect on the interpretation of bond strength measurements for this material system, but the alterations to matrix chemistry should not have changed the residual stress pattern, so that the observed effects are due to chemical bonding changes.

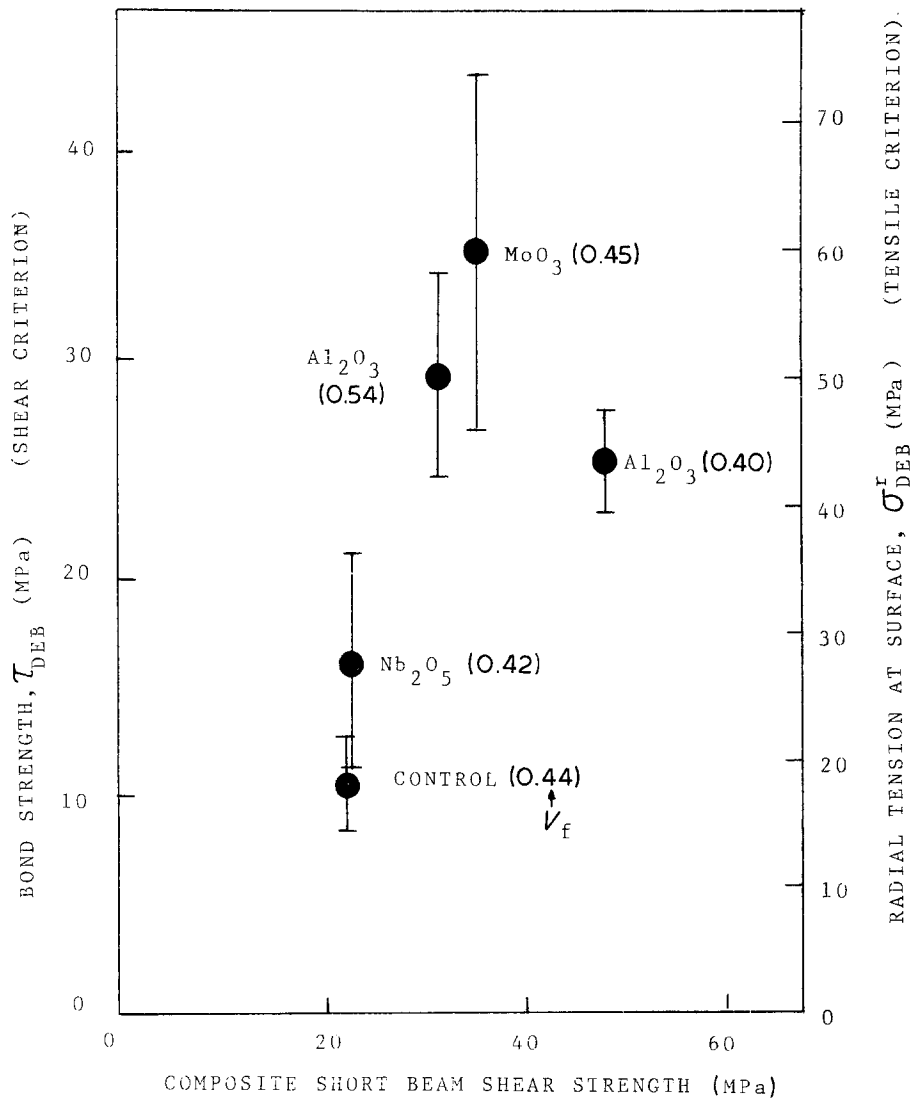


Figure 15 Effect of matrix modifications on bond strength and composite interlaminar shear strength for HMU carbon-borosilicate.

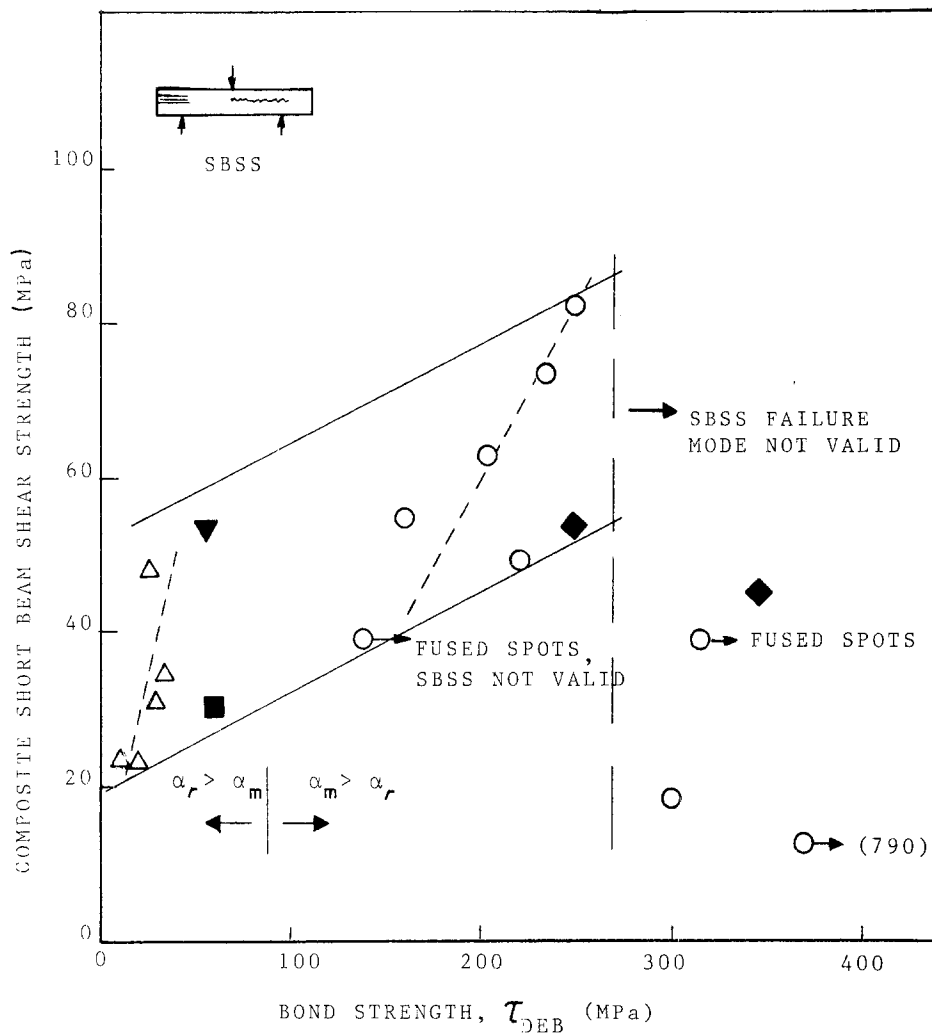


Figure 16 Composite interlaminar shear strength against bond strength (dashed lines indicate trends for individual material systems having varied chemical bonding). (■) Nicalon-BMAS; (○) Nicalon-1723 glass, effect of processing conditions; (◆) Nicalon-CAS I; (△) HMU-borosilicate, effect of matrix modifications; (▼) Nicalon-LAS III.

4.5. Correlations with thermal expansion mismatch and composite shear strength

The composite off-axis and shear strengths are critical properties in determining the damage-free working stress range for typical composite applications. As discussed earlier with reference to Fig. 1a, the fibre-matrix bond strength is expected to correlate with these composite properties, although many other factors may also be important including flaw size and fibre content, alignment and dispersion. Unidirectional composite shear strengths can be determined conveniently for cases which fail in a shear mode by the short-beam shear strength (SBSS) test (ASTM test method D4475) pictured in the inset of Fig. 16. The composite shear strength as determined in this test with a span-to-depth ratio of 5 is given for the Nicalon-reinforced systems in Fig. 16, along with the data from Fig. 15 for carbon-borosilicate. Failure did not always occur by a simple shear crack parallel to the fibres, and invalid tests are indicated, generally for those Nicalon-1723 systems in Fig. 11 with some interface regions having bond strengths above about 275 MPa. The failure modes for the CAS I and LAS III systems were transitional, with mixed compression and shear zones.

There is a general trend of higher composite shear strength with higher bond strength in Fig. 16. Stronger

trends are evident for the two systems with varying bond strength from changes in processing (Nicalon-1723) and matrix composition (carbon-borosilicate); the bond strength variations in both of these systems are due to changes in chemical bonding, since the thermal expansion coefficients are unaffected. For consistency, the calculated τ_{DEB} is used for the carbon-borosilicate system rather than the higher values for the radial tensile strength criterion. The data in Fig. 16 are clearly separated into two groups, those with $\alpha_r > \alpha_m$ having lower calculated bond strength, and those with $\alpha_m > \alpha_r$ having higher bond strength, where α_m and α_r are the matrix and radial fibre thermal expansion coefficients from Table I.

A nominal measure of the radial thermal residual stress (away from the free surface) can be taken as that for a single isotropic fibre embedded in a cylinder of matrix. In the limit of a very thick matrix layer, the nominal residual pressure at the interface, σ_{res}^r , is given by Southwell [38] (originally from Lamé in 1833) as

$$\sigma_{res}^r = (\alpha_m - \alpha_r)(-\Delta T)E_m \left/ \left[(1 + \nu_m) + (1 - \nu_r) \frac{E_m}{E_r} \right] \right. \quad (4)$$

where E_r and α_r are taken as the Young's modulus

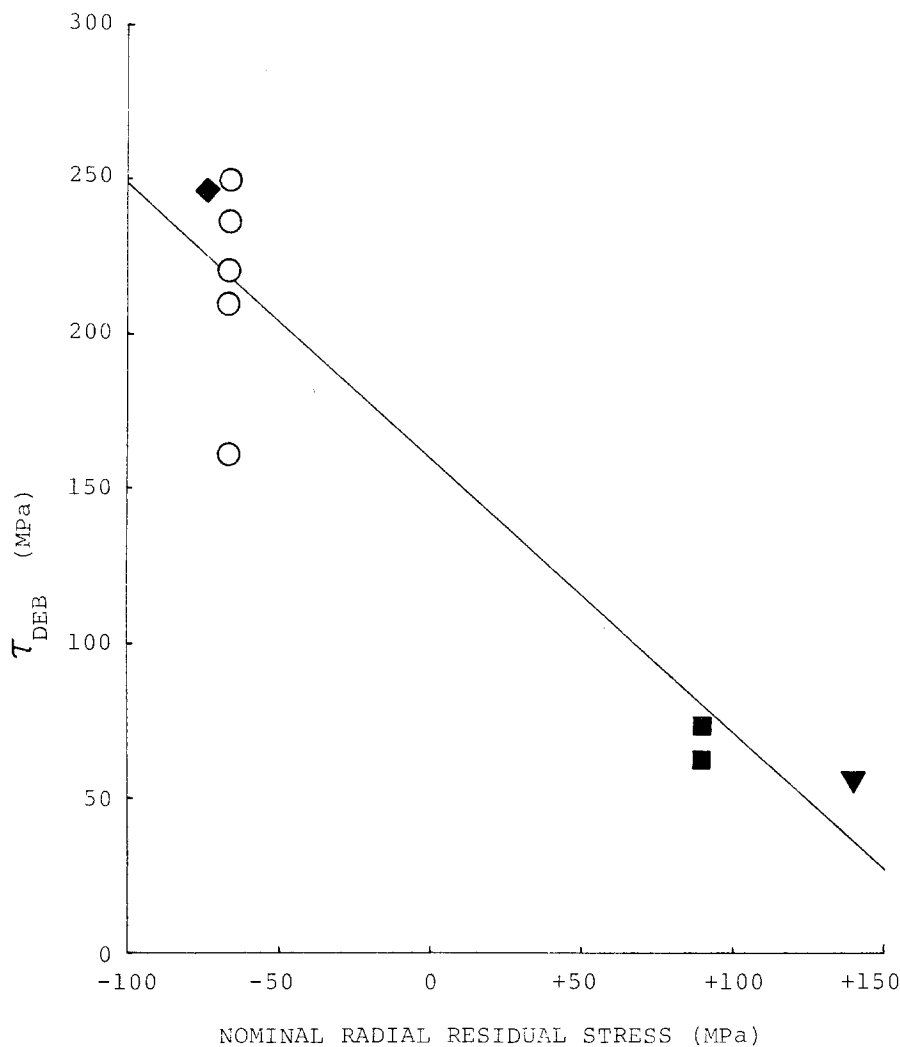


Figure 17 Bond strength against approximate nominal thermal residual interface stress in the radial direction for Nicalon-reinforced systems: (◆) CAS, (○) 1723, (■) BMAS III, (▼) LAS III.

and thermal expansion coefficient, respectively, of the fibre in the radial direction for carbon fibres. Fig. 17 gives the bond strength for the Nicalon-glass and glass-ceramic systems (processed under control conditions) plotted against the nominal residual stress. It should be noted that the residual stresses near the polished surface will be higher in most cases, and will include a significant residual shear stress (based on preliminary finite-element solutions). Furthermore, the radial residual stress on the interior will be affected by the discrete arrangement of neighbouring fibres, as solutions for fibre arrays have shown [39]; the sign of the residual stress can change in some fibre arrangements.

The results in Fig. 17 show the very significant effect of thermal residual stresses on bond strength measurements. If any chemical bond strength differences between the different materials in Fig. 17 are ignored, then the residual stress effect on the measurement is given approximately by the slope of the trend line

$$\tau_{DEB} = 160 - 0.89\sigma_{res} \quad (5)$$

Included in this effect is likely to be a coupling between the residual stress and the mechanical radial stress (Fig. 6). A residual compressive radial stress apparently permits the application of a higher mechanical probe force, which in turn generates an even higher radial compression, further suppressing bond failure. A more complete solution to the residual stress field and a better understanding of the effects of the radial stress magnitude on debonding are required

before an improved interpretation of these results is possible.

The results in Fig. 17 suggest a very strong influence of mechanical bonding effects on the measured bond strength. However, Figs 11, 13 and 15 indicate that similar or even greater variations are also possible from chemical bond changes in the absence of significant changes in residual stresses. Fig. 18 represents an attempt to offset the nominal residual stress effects evident in Figs 16 and 17 by shifting the bond data along the trend line in Fig. 17 (Equation 5) to coincide with the carbon-borosilicate residual stress value of (+) 58 MPa from Equation 4. This results in a shifted bond strength, τ_{DEB}^* , for the Nicalon systems following

$$\tau_{DEB}^* = \tau_{DEB} - 0.89(58 - \sigma_{res}^r) \quad (6)$$

Despite the uncertainties in bond strength interpretation which limit confidence in this treatment, Fig. 18 does appear to provide an improved correlation with the composite shear strength over Fig. 16, particularly for the systems where the chemical bonding was varied. This suggests that composite off-axis and shear strengths may be most strongly responsive to chemical rather than mechanical bond improvements, which is reasonable considering that the actual residual stress fields around fibres in closely packed regions may show very different values from Equation (4) [39].

The general trend of Fig. 18 is consistent with similar plots for carbon-epoxy composites [14], and a similar plot was given by Phillips [16] for carbon-

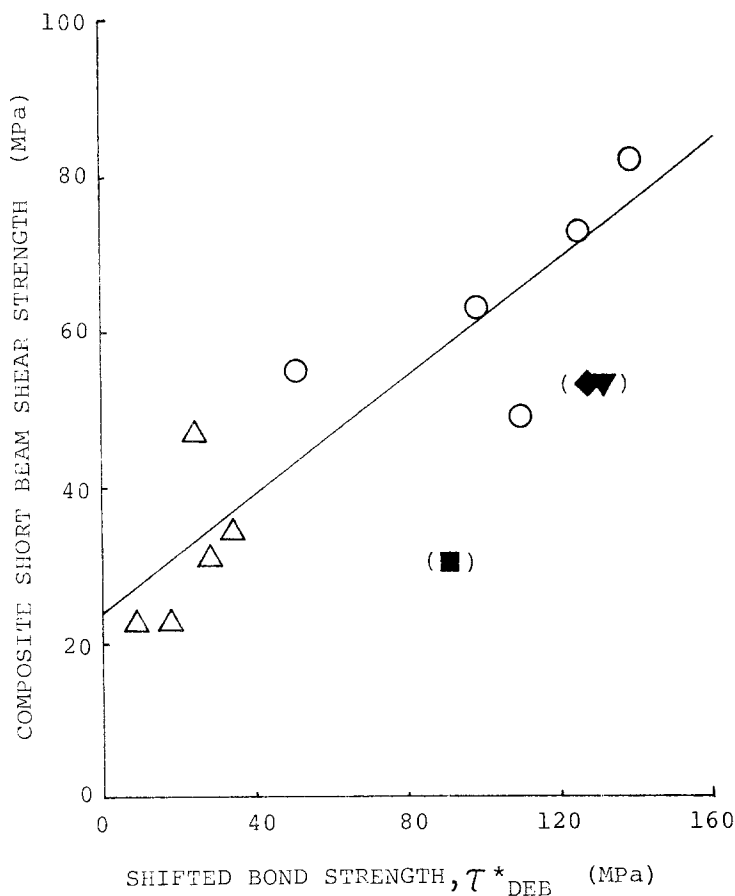


Figure 18 Composite short-beam shear strength against bond strength which has been shifted to offset nominal residual stress trend from Fig. 17, referenced to +58 MPa residual stress for carbon-borosilicate. (O) Nicalon-1723 glass, effect of processing conditions; (Δ) HMU-borosilicate, effect of matrix modifications; (\blacksquare) Nicalon-BMAS III; (\blacklozenge) Nicalon-CAS I; (\blacktriangledown) Nicalon-LAS III.

borosilicate and carbon-LAS, where the bond strength was deduced from work-of-fracture measurements. In the absence of any bond strength, the composite interlaminar shear strength (τ_{ILSS}) will still have a lower limiting value which can be approximated by a brittle matrix with cylindrical pores [40] (in the absence of larger flaws), giving approximately

$$\tau_{ILSS} = \left[1 - \left(\frac{4V_f}{\pi} \right)^{1/2} \right] \tau_m \quad (7)$$

where τ_m is the neat matrix shear strength. For a reasonable matrix shear strength of 100 MPa and a V_f of 0.40, Equation 7 gives a composite lower bound interlaminar shear strength of 29 MPa. This is in reasonable agreement with the intercept in Fig. 18. The curve fitted to the carbon-borosilicate and Nicalon-1723 system data for which the chemical bond strength was varied shows an increase in τ_{ILSS} with increasing bond strength of

$$\tau_{ILSS} = 23.8 + 0.38\tau_{DEB}^* \quad (8)$$

The individual Nicalon-glass-ceramic points fall to the right of the trend line fitted to glass matrix systems, possibly due to overshifting of the bond strengths from uncertainty about the coefficient of expansion data at high temperatures, or due to inherent effects of crystallization.

5. Conclusions

The microbonding test apparatus can be used to compressively load selected fibres in typical as-processed polymer, metal, and ceramic matrix composites to determine the force necessary to initiate debonding. In some cases the frictional sliding resistance of

debonded fibres can be determined by applying higher forces. A bond shear or tensile strength value can be calculated from a simplified micromechanics finite-element analysis, but further study is required to establish interface failure criteria and to include thermal residual stress effects.

The results indicate that very high bond strengths, above 500 MPa in the microdebonding test, cause weak, brittle composite behaviour in longitudinal tension and flexure. For bond strengths below 300 MPa, composites are strong and tough (as long as the fibres are not degraded during processing), and the tensile strength is not greatly affected by bond strength variations. Bond strengths above 500 MPa can result from strong bonding developed during processing in the absence of a weak interphase layer. Another cause of excessively strong bonding and embrittlement is oxidation of carbon interphase layers during high-temperature air exposure, if oxidation is followed by the formation of a new interphase layer with strong bonding, as with Nicalon-BMAS III.

Composites with strong, tough longitudinal properties still show a great deal of variation in off-axis and shear properties due to moderate changes in bond strength from variations in matrix chemistry or processing conditions. Increases in bond strength correlate with increases in composite interlaminar shear strength over a significant range, and the data suggest that chemical bonding is of the greatest importance. Residual stresses have a strong effect on the bond strength values determined with the microdebonding apparatus, but their significance (and that of other mechanical bonding effects) for composite behaviour can only be clarified through the development of

multiaxial interface failure criteria and improved analyses.

Acknowledgements

The test method and analysis development as well as studies of the carbon fibre systems were supported through the Office of Naval Research/Strategic Defense Initiative Office, Advanced Metal and Ceramic Matrix Composites Program at MIT. Additional support, materials supply, property data, and helpful discussion were provided through K. Chyung at Corning Glass Works, and the high-temperature testing was supported by NASA-Lewis Research Center. Carbon-borosilicate samples and interlaminar shear strength data were provided by K. Prewo of United Technologies Research Center. Analysis of the transversely isotropic Hertzian problem and assistance with the finite-element solutions were provided by S.-H. Jao.

References

1. M. J. KLEIN, in "Composite Materials", Vol. 1: Interfaces in Metal Matrix Composites, edited by A. G. Metcalf, L. J. Broutman and R. H. Krock (Academic, New York, 1974) p. 169.
2. A. E. NAAMAN, A. S. ARGON and F. MOAVEN-ZADEH, *Cement Concr. Res.* **3** (1973) 397.
3. L. J. BROUTMAN and F. J. MCGARRY, in "Proceedings of 17th Conference of SPI Reinforced Plastics Division" Chicago, 1962 (Society of the Plastics Industry, New York, 1962) Paper 1-E.
4. L. PENN and S. M. LEE, *Fibre Sci. Tech.* **17** (1982) 91.
5. B. MILLER, presentation at NASA workshop on Carbon Fiber Surface Properties and Adhesion, NASA-Langley Research Center, Hampton, Virginia, December 1985.
6. R. D. MOONEY and F. J. MCGARRY, in Proceedings of 14th Conference of SPI Reinforced Plastics Division" Chicago, 1959 (Society of the Plastics Industry, New York, 1959) Paper 12-E.
7. J. AVESTON, G. A. COOPER and A. KELLY, in Proceedings of Conference on Fibre Composites, National Physical Laboratory, Teddington, England, 1971 (IPC Service and Technology Press, Guildford, 1971) p. 15.
8. L. T. DRZAL, *SAMPLE J.* **19** (1983) 7.
9. D. B. MARSHALL, *Commun. Amer. Ceram. Soc.* **67** (1984) C259.
10. B. BUDIANSKY, J. W. HUTCHINSON and A. G. EVANS, *J. Mech. Phys. Solids* **34** (1986) 167.
11. D. B. MARSHALL and W. C. OLIVER, *J. Amer. Ceram. Soc.* **70** (1987) 542.
12. J. F. MANDELL, D. H. GRANDE, T. H. TSAING and F. J. MCGARRY, ASTM STP 893 (American Society for Testing and Materials, Philadelphia, 1986) p. 87.
13. J. F. MANDELL, J. H. CHEN and F. J. MCGARRY, in Proceedings of 35th Conference of R.P./Composite Institute New Orleans 1980 (Society of the Plastics Industry, New York, 1980) Paper 26D.
14. L. YING, in Proceedings of 35th Conference, R.P./Composites Institute New Orleans, 1980 (Society of the Plastics Industry, New York, 1983) Paper 20-C.
15. L. J. EBERT and P. K. WRIGHT, in "Composite Materials," Vol. 1: Interfaces in Metal Matrix Composites, edited by A. G. Metcalf, L. J. Broutman and R. H. Krock (Academic, New York, 1974) p. 31.
16. D. C. PHILLIPS, *J. Mater. Sci.* **9** (1974) 1847.
17. D. C. PHILLIPS, R. A. SAMBELL and D. H. BOWEN, *ibid* **7** (1972) 1454.
18. J. F. MANDELL, D. H. GRANDE and J. JACOBS, ASME Gas Turbine Conference and Exhibit, Anaheim, June 1987. Trans. ASME, *J. of Engr. for Gas Turbines and Power*, **109** (1987) 267.
19. K. M. PREWO and V. C. NARDONE, Report R86-917161-1, (United Technologies Research Center, East Hartford, Connecticut, 1986).
20. D. H. GRANDE, MS thesis, Massachusetts Institute of Technology (1983).
21. *Idem*, PhD thesis, Massachusetts Institute of Technology (1987).
22. J. W. LAUGHNER, N. J. SHAW, R. T. BHATT and J. A. DiCARLO, presented at 10th Annual Conference on Composites and Advanced Ceramic Materials, American Ceramics Society, Coco Beach, Florida, 1986.
23. T.-H. TSAING, ScD thesis, Massachusetts Institute of Technology (1983).
24. K. CHYUNG, personal communication (1987).
25. C. C. CHAMIS, in Proceedings of 39th Conference, RP/Composites Institute Houston, 1984 (Society of the Plastics Industry, New York, 1984) Paper 11-D.
26. K. M. PREWO, J. J. BRENNAN and G. K. LAYDEN, *Ceram. Bull.* **65** (1986) 305.
27. R. F. COOPER and K. CHYUNG, presented at American Ceramics Society, 88th Annual Meeting, Chicago, 1986.
28. R. L. STEWART, K. CHYUNG, M. P. TAYLOR and R. F. COOPER, in "Fracture Mechanics of Ceramics", Vol. 7, edited by R. C. Brandt, A. G. Evans, D. P. H. Hasselman and F. F. Lange (Plenum, New York, 1986) p. 33.
29. S. TIMOSHENKO and J. N. GOODIER, "Theory of Elasticity" (McGraw-Hill, New York, 1951) p. 362.
30. S. G. LEKHNITSKII, "Theory of Elasticity of an Anisotropic Elastic Body" (Holden-Day, San Francisco, 1963) p. 347.
31. K. M. PREWO and G. K. LAYDEN, Report R84-916175-1 (United Technologies Research Center, East Hartford, Connecticut, 1984).
32. D. B. MARSHALL and A. G. EVANS, *J. Amer. Ceram. Soc.* **68** (1985) 225.
33. M. TAYLOR, presented at American Ceramics Society, 88th Annual Meeting, Chicago, 1986.
34. K. M. PREWO, *J. Mater. Sci.* **21** (1986) 3590.
35. E. Y. LUH and A. G. EVANS, *Ceram. Eng. Sci. Proc.* **6** (1985) 608.
36. T.-I. MAH, Presented at American Ceramics Society 88th Annual Meeting, Chicago, 1986.
37. T. W. COYLE, A. GILAT, S. W. FREIMAN and E. R. FULLER Jr, Materials Research Society Fall Meeting, Boston, 1986.
38. R. V. SOUTHWELL, "An Introduction to the Theory of Elasticity for Engineers and Physicists" (Oxford University Press, London, 1941) p. 406.
39. C. C. CHAMIS, in "Composite Materials", Vol 6; Interfaces in Polymer Matrix Composites, edited by E. P. Plueddemann, L. J. Broutman and R. H. Krock (Academic, New York, 1974) p. 31.
40. L. B. GRESZCZUK, in "Proceedings of 22nd Reinforced Plastics Division Meeting Washington DC, 1967 (Society of the Plastics Industry, New York, 1967) Paper 20-A.

Received 30 March
and accepted 8 June 1987